Electrical Power and Energy Systems 101 (2018) 92–102

Contents lists available at ScienceDirect

Electrical Power and Energy Systems

journal homepage: www.elsevier.com/locate/ijepes

Nonlinear predictive control of a DFIG-based wind turbine for power capture optimization

A. Bektache[a], B. Boukhezzar[b]

[a] Ferhat Abbas university Sétif 1, Cité Maabouda, 19000 Setif, Algeria
[b] Laboratoire d'Automatique et de Robotique de Constantine, Mentouri brothers university, Route de Aïn-el-Bey, 25000 Constantine, Algeria

ARTICLE INFO

Keywords:
Wind turbine
Doubly fed induction generator (DFIG)
Nonlinear control
Predictive control
Power capture optimization

ABSTRACT

A nonlinear predictive controller is proposed for a variable speed wind turbine. The objective is power capture optimization and transient loads reduction. The controller acts only on low wind speed area. It consists of a doubly fed induction generator controller coupled with a model predictive aeroturbine controller. Unlike the majority of existing work on DFIG, the nonlinear controller deals directly with the generator model without any simplifying assumptions. This makes it possible to remove some assumptions on the DFIG model. The nonlinear DFIG controller achieves asymptotic torque and flux tracking. For the aeroturbine part, the model predictive controller uses predictions of the output to compute the optimal control sequence. It makes a compromise between power capture optimization and loads reduction. The controllers design procedure is detailed. The global controller is tested with the parameters of a real experimental variable speed wind turbine. It is compared with PID and LQG controllers. The simulations show satisfactory results in comparison with these schemes. The proposed controller achieves better power capture optimization and load reduction. It therefore allows a good achievement of the design objectives.

1. Introduction

Control design is a key factor for variable speed wind turbine (VSWT) efficiency enhancement [1]. During the last decades, a considerable amount of literature has been devoted to wind turbines control design. A substantial review of this literature is given from [2] to [3]. A wide variety of advanced control strategies has been applied to VSWT control either in low or high wind speed areas [4]. In general terms, the dedicated literature to wind turbine control can be split in many parts:

1. The first one concerns aeroturbine control. Only the mechanics and aerodynamics of the turbine are considered. The electric generator and power converters models are not considered. It is then assumed that the control inputs are directly the pitch angle and the generator torque [5]. The main control objective in this case is either wind power capture optimization for low wind speeds or electrical power and rotor speed regulation for high wind speed. Almost all classical linear control techniques have been applied to this control problem. PI/PID controllers [6], state space based LQ/LQG controllers [7] linear $\mathscr{H}_\infty$ controllers [8] are widely used. More recently, gain scheduling controllers [9,10]. However, a simple linear wind turbine controller achieves poor dynamic performances. Such a controller can not deal with strong nonlinear aerodynamics and highly turbulent wind. To overcome this limitation, self-tuning regulators, adaptive linear regulators [11,12] and gain-scheduling ones [10] are proposed. In order to take directly into consideration the nonlinear model of the aeroturbine, several nonlinear controllers have been proposed [13]. The main drawback of these techniques is the complexity of the controller. However, the high computing power of recent calculator devices makes the implementation of nonlinear controllers possible.
2. The second part of the literature dedicated to wind turbine control considers a very simplified model of the wind and the aeroturbine. On the other hand, a detailed dynamic model of the electric generator is considered. Generally, the generator model is a two reference frame model ($d-q$,$\alpha-\beta$). It is obtained using a Park transformation of the generator equations [14]. The control objectives are mainly the control of the active P and reactive Q electrical power. The main considered topology is a variable speed wind turbine equipped with a DFIG generator. This one is fed by a two side PWM back-to-back converters [15]. Different control strategies are used. Classical ones use vector field-oriented control. The stator or rotor flux are then oriented along the d axis [16]. More advanced control strategies use nonlinear control [17], adaptive control [18], sliding mode control [19] and backstepping [20]. These control

E-mail addresses: bektachedz@yahoo.fr (A. Bektache), boubekeur.boukhezzar@umc.edu.dz (B. Boukhezzar).

https://doi.org/10.1016/j.ijepes.2018.03.012
Received 3 April 2017; Received in revised form 8 February 2018; Accepted 10 March 2018

Nomenclature

v	wind speed, m·s^{-1}
ρ_{air}	air density, kg·m^{-3}
R	rotor radius, m
P_a	aerodynamic power, W
T_a	aerodynamic torque, N·m
$T_{a_{hs}}$	high-speed equivalent aerodynamic torque, N·m
$E_{aero}(\%)$	aerodynamic efficiency, (%)
λ	tip speed ratio
β_p	pitch angle, deg
$C_p(\lambda,\beta_p)$	power coefficient
$C_q(\lambda,\beta_p)$	torque coefficient
ω_t	rotor speed, rad·s^{-1}
ω_g	generator speed, rad·s^{-1}
ω_{ls}	low speed shaft speed, rad·s^{-1}
θ_t	rotor side angular deviation, rad
θ_{ls}	gearbox side angular deviation, rad
θ_g	generator side angular deviation, rad
T_{em}	generator (electromagnetic) torque, N·m
T_{ls}	low speed shaft torque, N·m
T_{hs}	high speed shaft torque, N·m
J_r	rotor inertia, kg·m^2
J_g	generator inertia, kg·m^2
$J_{t_{hs}}$	high-speed equivalent inertia, kg·m^2
K_r	rotor external damping, N·m·rad^{-1}·s^{-1}
K_g	generator external damping, N·m·rad^{-1}·s^{-1}
K_{ls}	low speed shaft damping, N·m·rad^{-1}·s^{-1}
$K_{t_{hs}}$	high-speed equivalent damping, N·m·rad^{-1}·s^{-1}
B_{ls}	low speed shaft stiffness, N·m·rad^{-1}
n_g	gearbox ration,
ϕ_{sd}	direct axis stator flux, Wb
ϕ_{sq}	quadrature axis stator flux, Wb
i_{rd}	direct axis rotor current, A
i_{rq}	quadrature axis rotor current, A
v_{sd}	direct axis stator voltage, V
v_{sq}	quadrature axis stator voltage, V
v_{rd}	direct axis rotor voltage, V
v_{rq}	quadrature axis rotor voltage, V
ρ	(d,q) reference frame position, rad
p	number of pole pairs,
M	mutual inductance, H
ε_i	tracking error,
WT	Wind Turbine
VSWT	Variable Speed Wind Turbine
DFIG	Doubly Fed Induction Generator

strategies give good performances. However, they are generally complex to be implemented. Add to this, in many works, the control strategies are tested under unrealistic conditions. Constant wind speed profile or untested aerodynamic wind turbine characteristics are often used for these tests [21].

In this work, a whole nonlinear model is considered for both the DFIG and the aeroturbine. This makes it possible to have a model closer to physical reality. For control objectives, it is desirable to use a control technique which ensures a good compromise between efficiency and complexity. Predictive control is a well known control strategy. It has been used and implemented in many industrial applications (chemical process, metallurgy, paper industry, aerospace and automotive control [22].) Predictive control also has got a great importance in application to wind energy. A review of the predictive control of VSWT is presented in [23]. However, in many works on predictive control of VSWT, the suggested controllers consider only the generator control [24–26] or the aeroturbine control [27,28,7]. It is important to consider both of them together. The new feature of this work is that the presented controller deals either with the generator or with the aeroturbine control. Contrarily to many other works, no simplifying assumptions are made to the DFIG model. In many control schemes in the literature, simplified models are used for the generator for control design [29,30]. Under some conditions, these assumptions can not be maintained. An interesting approach is proposed in [31] using nonlinear model predictive direct power control (PDPC). The aim of this approach is to control the active and reactive power of a DFIG wind turbine. A constrained objective function is adopted to reduces active and reactive power ripples. An optimization algorithm is then used to compute the control actions. In this article, the objective is to optimize aerodynamic power capture. It is a different objective than active and reactive power regulation as done in [31]. A quadratic programming algorithms are used instead of nonlinear multi objective optimization used in [31].

In this work, the whole nonlinear model of the DFIG is used for the design of a nonlinear state feedback controller. This provides a controller that can overcome the simplifying assumptions. The proposed controller acts only on low wind speed region. A whole controller is to be considered in future works. It should cover all the operating area including low and high wind speed regions.

This paper is organized as follows: First, the aeroturbine nonlinear one-mass model is deduced in Section 2. After that, the state-space representation of the DFIG used for the controller design is given. At the end of this section, the objectives of the VSWT control are detailed. A special focus is accorded to the low wind speed area and power capture optimization. The proposed controller is detailed in Section 3 in three steps: Firstly, the nonlinear DFIG state feedback with asymptotic output tracking is deduced. The objective is to track the electromagnetic torque and stator flux references. Secondly, a multi-criteria model predictive controller (MPC) is obtained. The aim is tracking the optimal wind turbine speed to maximize wind power capture. Finally, the scheme of the global controller is presented and the interconnection between the sub-controllers is explained. Section 4 presents the simulation results obtained with the controllers. Real parameters of an experimental wind turbine are used. A conclusion and perspectives are then drawn. Some calculus details and the wind turbine parameters are given in appendixes.

2. Wind turbine modeling

The considered wind turbine in this work is an experimental medium-scale variable speed wind turbine. It is equipped with a doubly fed induction generator associated with a two side back-to-back converter. This configuration is depicted in Fig. 1. This is a common variable speed wind turbine scheme [6]. The used model for controllers design includes the aeroturbine and the generators models.

2.1. Aeroturbine modeling

The mechanical structure of a wind turbine is modeled as a flexible interconnection of rigid rotating mass. Many models are suggested in the literature using one, two or multiple mass [32,33]. A two-mass model is commonly used as a good compromise between efficiency and simplicity. A two-mass model is composed of two rotating inertias connected by a flexible shaft and a gearbox [34]. The gearbox connects the aerodynamic rotor shaft side (low speed side) to the generator shaft side (high speed shaft). From Fig. 2 diagram, the mechanical equation of a two-mass wind turbine model is given by

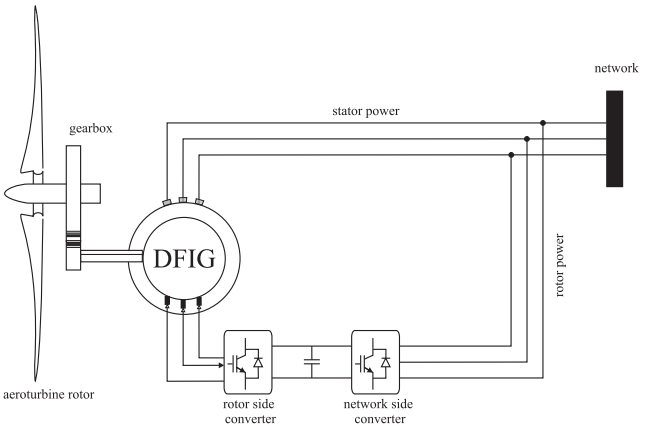

Fig. 1. Wind turbine with converters and generator scheme.

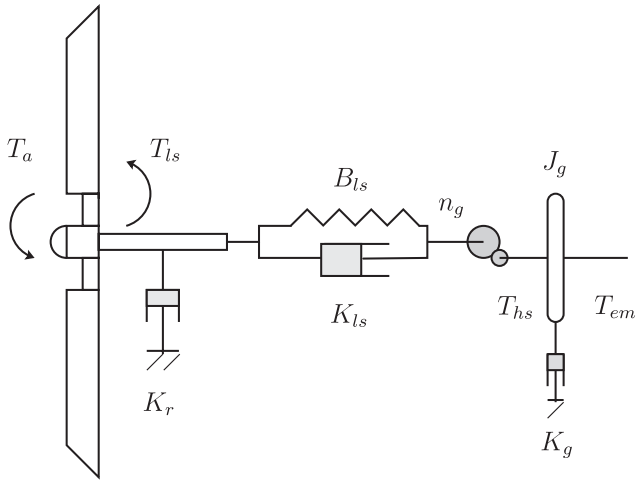

Fig. 2. Two-mass wind turbine model.

$$\begin{cases} J_r\dot{\omega}_t = T_a - T_{ls} - K_r\omega_t \\ T_{ls} = B_{ls}(\theta_t - \theta_{ls}) + K_{ls}(\omega_t - \omega_{ls}) \\ J_g\dot{\omega}_g = T_{hs} - K_g\omega_g - T_{em} \end{cases} \tag{1}$$

As shown in Fig. 2, J_r,K_r and J_g,K_g are respectively low-speed and high-speed inertia and viscous friction and n_g is the gearbox coefficient. See Fig. 2 and the nomenclature section for the significance of the variables. The gearbox ratio n_g links the low speed shaft variables to the high speed ones as follows

$$n_g = \frac{T_{ls}}{T_{hs}} = \frac{\omega_g}{\omega_{ls}} = \frac{\theta_g}{\theta_{ls}} \tag{2}$$

The aerodynamic torque T_a is a nonlinear function. It is proportional to the square of the effective wind speed v^2 via the torque coefficient $C_q(\lambda,\beta_p)$

$$T_a(\omega_t, v, \beta_p) = \frac{1}{2}\rho_{air}\pi R^3 C_q(\lambda,\beta_p)v^2 \tag{3}$$

The torque coefficient $C_q(\lambda,\beta_p)$ is a nonlinear function of the pitch angle β_p and the tip-speed ratio λ

$$\lambda = \frac{\omega_t R}{v} \tag{4}$$

where ω_t is the rotor speed, R is the rotor radius and ρ_{air} is the air density.

The aerodynamic torque T_a is connected to the aerodynamic power by the relation

$$P_a = T_a\omega_t \tag{5}$$

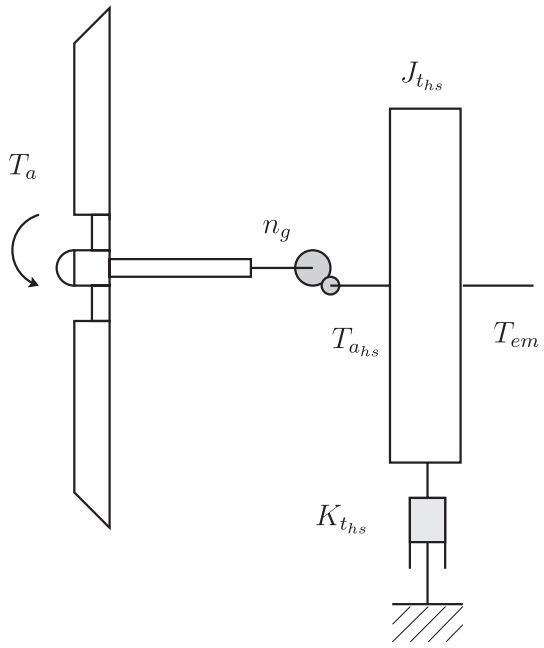

Fig. 3. One-mass wind turbine model in the high-speed shaft side.

the aerodynamic power is also expressed a follows

$$P_a = \frac{1}{2}\rho_{air}\pi R^2 C_p(\lambda,\beta_p)v^3 \tag{6}$$

with

$$C_p(\lambda,\beta) = \lambda C_q(\lambda,\beta_p) \tag{7}$$

the relation between the aerodynamic torque and aerodynamic power coefficients.

In order to simplify the two-mass model, a perfect rigid low speed shaft is assumed. It is then possible to brought all the variables to one side: high-speed or low-speed side. A one-mass model is then obtained. In this work, the aeroturbine is modeled as a one-mass rotating inertia. All the variables are brought to the high-speed side (generator side) [5,35]. This is motivated by the need for a reduced whole model complexity including generator and aeroturbine models. Add to this, as the generator is in the high-speed side, a high-speed shaft equivalent is appropriate. As shown in Fig. 3, the one-mass high-speed equivalent model can be schematized as an equivalent inertia J_{hs}. It is driven by a high-speed equivalent aerodynamic torque $T_{a_{hs}}$ and braked by the generator electromagnetic torque T_{em} and a viscous friction torque. This last one is proportional to the generator speed ω_g with a coefficient $K_{t_{hs}}$. The mechanical equation is therefore

$$J_{t_{hs}}\dot{\omega}_g = T_{a_{hs}} - K_{t_{hs}}\omega_g - T_{em} \tag{8}$$

The hight-speed equivalent variables are deduced by bringing all the low-speed side (aerodynamic rotor side) to the high-speed side. The low-speed side variables are rescaled when transferred to the high-speed shaft [5]

$$\begin{aligned} T_{a_{hs}} &= \frac{T_a}{n_g} \\ J_{t_{hs}} &= J_g + \frac{J_r}{n_g^2} \\ K_{t_{hs}} &= K_g + \frac{K_r}{n_g^2} \end{aligned} \tag{9}$$

where $T_{a_{hs}}$,$J_{t_{hs}}$ and $K_{t_{hs}}$ are respectively the high-speed side equivalent aerodynamic torque, inertia and viscous frictions coefficient.

2.2. Generator modeling

Different generator models are used for variable speed wind turbines [6,36]. The doubly fed induction generator (DFIG) converter is a common and efficient configuration. It is associated with a back-to-back voltage source [37,15]. In this paper, in order to reduce the controller complexity, only the DFIG model is considered. The power converter model and controller will not be considered. This is justified by the very fast dynamics of the controlled converter compared to the DFIG dynamics [38]. In fact, much work has been devoted to the power converters control [39,40]. Efficient controllers with a very fast time response were developed. Either with classical [41] or advanced controllers [42], it is possible to achieve an efficient regulation of AC/DC/AC converters. Their output currents and voltages can then reach their references with a settling time around 1 ms. As the DFIG is fed by the power converter, the DFIG-converter control system has a cascade control structure [43]. The power converter control loop is within the DFIG control loop. The controlled power converter has a settling time around 1 ms and the desired settling time of the DFIG is of the order of 10 ms. The power converter control loop can then be seen as a static system. One can assume that the voltage reference and the power converter output are the same.

The DFIG is modeled in a rotating (d,q) frame linked to the stator flux vector [15,44]. The stator flux vector coincides with the d axis giving

$$\phi_{sd} = \phi_s; \qquad \phi_{sq} = 0 \tag{10}$$

The state space representation of the DFIG in this frame is given by the following system of equations [44]

$$\begin{cases} \frac{d\omega_g}{dt} = -\mu\phi_{sd} i_{rq} - \frac{K_t}{J_t}\omega_g + T_{a_{hs}} \\ \frac{d\phi_{sd}}{dt} = -\alpha\phi_{sd} + M\alpha i_{rd} + v_{sd} \\ \frac{d\varphi}{dt} = \frac{M\alpha i_{rq} + v_{sq}}{\phi_{sd}} \\ \frac{di_{rd}}{dt} = \alpha\beta\phi_{sd} - \gamma i_{rd} + \frac{M\alpha i_{rq}^2}{\phi_{sd}} + \frac{i_{rq} v_{sq}}{\phi_{sd}} - p\omega_g i_{rq} - \beta v_{sd} + \frac{1}{\sigma} v_{rd} \\ \frac{di_{rq}}{dt} = \beta p\omega_g \phi_{sd} - \frac{M\alpha i_{rd} i_{rq}}{\phi_{sd}} - \frac{i_{rd} v_{sq}}{\phi_{sd}} + p\omega_g i_{rd} - \gamma i_{rq} - \beta v_{sq} + \frac{1}{\sigma} v_{rq} \end{cases} \tag{11}$$

with

$$\sigma = L_r\left(1 - \frac{M^2}{L_r L_s}\right), \quad \alpha = \frac{R_s}{L_s}$$
$$\beta = \frac{M}{\sigma L_s}, \quad \gamma = \frac{R_r}{\sigma} + \beta\alpha M$$
$$M = \frac{M}{J_t L s},$$

The considered state variables are the generator speed ω_g, the $d-$axis stator flux ϕ_{sd}, the (d,q) frame angle ρ and the rotor currents i_{rd} and i_{rq}

$$x = [\omega_g \quad \phi_{sd} \quad \rho \quad i_{rd} \quad i_{rq}]^T$$

There are five input variables: The high-speed side aerodynamic torque $T_{a_{hs}}$, the stator frame voltages v_{sd} and v_{sq} and the rotor frame voltages v_{rd} and v_{rq}. As the DFIG is controlled from the rotor side converter, only the rotor voltages v_{rd} and v_{rq} are effective control inputs.

2.3. Power capture optimization

As shown in Fig. 4, a wind turbine is operational if the wind speed is situated in the interval $[v_{min}, v_{max}]$. In zone I, the control objective is to optimize the wind power capture. The aerodynamic coefficient $C_p(\lambda,\beta_p)$ should be maintained at its unique optimal value. The tip speed ratio λ and the pitch angle β_p should therefore be fixed to their optimal values

$$\lambda = \lambda_{opt} \tag{12}$$

$$\beta_p = \beta_{p_{opt}} \tag{13}$$

such that

$$C_p(\lambda_{opt},\beta_{p_{opt}}) = C_{p_{opt}} \tag{14}$$

In order to fix the tip speed ration to its optimal value, the rotor speed ω_t should track the optimal rotor speed $\omega_{t_{opt}}$ given by

$$\omega_{t_{opt}} = \frac{\lambda_{opt}}{R} v \tag{15}$$

the optimal rotor speed is proportional to the wind speed. However, in order to alleviate high loads and control effort, it is not convenient to make a close tracking of the wind speed turbulence. A good controller should track the mean tendency of the optimal rotor speed profile $\omega_{t_{opt}} = \frac{\lambda_{opt}}{R} v$. This profile has the same shape as the wind speed ones. A compromise is then made between power capture enhancement and loads reduction. This is obtained by an appropriate choice of the controller bandwidth.

The power and rotor speed regulation for high wind speeds are not tackled in this paper. The proposed controller acts in the low wind speed area for power capture optimization. It is a common way to do even in recent works [45,46]. A whole controller is to be considered in future works. It should include full load area for high wind speed (region III in Fig. 4). It should also take into consideration the transition region II between power capture optimization (region I) and power regulation (region III).

3. Nonlinear predictive wind turbine controller

The nonlinear predictive controller presented in this section is composed of two cascaded controllers: A DFIG controller in the internal loop and an MPC aeroturbine controller in the external loop.

3.1. Nonlinear asymptotic output tracking DFIG controller

A considerable bibliography is devoted to the DFIG control. Classical techniques such as vector control with PI controllers were widely used [47]. In order to apply a design procedure similar to the induction machine control ones, many assumptions are made. Some authors neglect the rotor and stator transients [48]. Others consider that the rotor currents are well controlled [49]. It is also assumed that the stator resistance voltage loss is neglected [30]. A reduced order of the DFIG is then used for the controller design. In this work, the detailed model of the DFIG is used without any simplification. A nonlinear controller is then designed.

Lets consider a square nonlinear system with m inputs and m outputs. The aim of a nonlinear state feedback controller is to transform the nonlinear system to a linear one. The obtained linear system has new inputs $v_i, 1 \leqslant i \leqslant m$. Each input is linked to one output via an r_i-integrator linear transfer function. The integer r_i is the partial relative

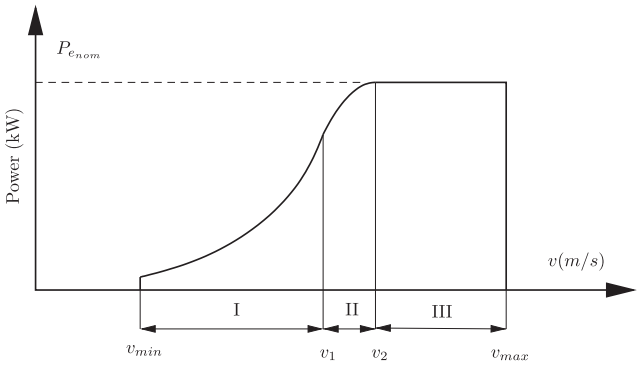

Fig. 4. Wind turbine power curve.

degree of the i^{th} output [50]. In the case of the DFIG, the considered outputs are the stator flux $y_1 = \phi_s$ and the electromagnetic torque $y_2 = T_{em}$. In order to compute the relative degree of the two outputs, each one is derivated with respect to time. The derivation stops when a control input appears explicitly. Lets first consider the relative degree of the stator flux $\phi_s = \phi_{sd}$. Its first derivative is directly given by the DFIG Section 4.2

$$\frac{d\phi_s}{dt} = -\alpha\phi_{sd} + M\alpha i_{rd} + v_{sd} \tag{16}$$

the second time derivative of ϕ_s is then

$$\frac{d^2\phi_s}{dt^2} = -\alpha\frac{d\phi_{sd}}{dt} + M\alpha\frac{di_{rd}}{dt} + \frac{dv_{sd}}{dt} \tag{17}$$

by replacing $\frac{d\phi_{sd}}{dt}$ and $\frac{di_{rd}}{dt}$ by their expressions given in (11) one obtains

$$\frac{d^2\phi_s}{dt^2} = -\alpha[-\alpha\phi_{sd} + M\alpha i_{rd} + v_{sd}] + M\alpha\left[\alpha\beta\phi_{sd} - \gamma i_{rd} + \frac{M\alpha i_{rq}^2}{\phi_{sd}} + \frac{i_{rq}}{\phi_{sd}}v_{sq} - p\omega_g i_{rq} - \beta v_{sd} + \frac{1}{\sigma}v_{rd}\right] + \frac{dv_{sd}}{dt} \tag{18}$$

Therefore, the stator flux has a relative degree $r_1 = 2$. It can be controlled by the v_{rd} input. The details of stator voltage direct component time derivative $\frac{dv_{sd}}{dt}$ is given in Appendix B.

Considering now the relative degree of the electomagnetic torque T_{em}

$$T_{em} = -p\frac{M}{L_s}\phi_{sd}i_{rq} \tag{19}$$

Its first time derivative is given by

$$\frac{dT_{em}}{dt} = -p\frac{M}{L_s}\frac{d\phi_{sd}}{dt}i_{rq} - p\frac{M}{L_s}\phi_{sd}\frac{di_{rq}}{dt} \tag{20}$$

substituting $\frac{d\phi_{sd}}{dt}$ and $\frac{di_{rq}}{dt}$ by their expressions in Eq. (11) gives

$$\frac{dT_{em}}{dt} = -p\frac{M}{L_s}[-\alpha\phi_{sd} + M\alpha i_{rd} + v_{sd}]i_{rq} - p\frac{M}{L_s}\phi_{sd}v\left[\beta p\omega_g\phi_{sd} - \frac{M\alpha i_{rd}i_{rq}}{\phi_{sd}} - \frac{i_{rd}}{\phi_{sd}}v_{sq} + p\omega_g i_{rd} - \gamma i_{rq} - \beta v_{sq} + \frac{1}{\sigma}v_{rq}\right] \tag{21}$$

As the control input v_{rq} is included in the first derivative of T_{em}, the electromagnetic torque T_{em} has a relative degree $r_2 = 1$. It is controlled by the input voltage v_{rq}.

In order to linearize the DFIG by a nonlinear state feedback, one has to find the two control inputs v_{rd} and v_{rq}. They are chosen such that the close-loop systems behave like two linear independent systems. Each system has respectively new input u_d and u_q. They are described by the following linear differential equations

$$\frac{d^2\phi_s}{dt^2} = u_d \tag{22}$$

and

$$\frac{dT_{em}}{dt} = u_q \tag{23}$$

by combining Eqs. (22), (23) with (18), (21), the linearizing control inputs are given by

$$v_{rd} = \frac{\sigma}{M\alpha}\left[-M\alpha\left(\alpha\beta\phi_{sd} - \gamma i_{rd} + \frac{M\alpha i_{rq}^2}{\phi_{sd}} + \frac{i_{rq}v_{sq}}{\phi_{sd}} - p\omega_g i_{rq} - \beta v_{sd}\right) + \alpha(-\alpha\phi_{sd} + M\alpha i_{rd} + v_{sd}) - \frac{dv_{sd}}{dt} + u_d\right] \tag{24}$$

and

$$v_{rq} = -\frac{\sigma L_s}{pM\phi_{sd}}\left[\frac{pM}{L_s}\phi_{sd}\left(\beta p\omega_g\phi_{sd} - \frac{M\alpha i_{rd}i_{rq}}{\phi_{sd}} - \frac{i_{rd}v_{sq}}{\phi_{sd}} + p\omega_g i_{rd} - \gamma i_{rq} - \beta v_{sq}\right) + \frac{pM}{L_s}(-\alpha\phi_{sd} + M\alpha i_{rd} + v_{sd})i_{rq} + u_q\right] \tag{25}$$

A stable dynamics are imposed to the stator flux and electromagnetic tracking errors. As the relative degree of the stator flux ϕ_s is $r_1 = 2$, a second order dynamic is imposed to the stator flux tracking error ε_1

$$\ddot{\varepsilon}_1 + a_1\dot{\varepsilon}_1 + a_0\varepsilon_1 = 0 \tag{26}$$

with

$$\varepsilon_1 = \phi_s - \phi_{s_{ref}} \tag{27}$$

and

$$s^2 + a_1 s + a_0 \tag{28}$$

a Hurwitz stable polynomial. The choice of tuning parameters a_0 and a_1 is detailed in Appendix C. By merging Eq. (22) with Eqs. (26) and (27) and substituting $\frac{d\phi_{sd}}{dt}$ by its expression given in Eq. (11), the new control input u_d is given by

$$u_d = \ddot{\phi}_{s_{ref}} - a_1(-\alpha\phi_{sd} + M\alpha i_{rd} + v_{sd} - \dot{\phi}_{s_{ref}}) - a_0(\phi_{sd} - \phi_{s_{ref}}) \tag{29}$$

and the final expression of v_{rd} is deduced by replacing u_d in Eq. (24) by the above expression (29).

As shown previously, the relative degree of the electromagnetic torque T_{em} is one. An asymptotically stable first order dynamic is then imposed to the aerodynamic torque tracking error ε_2.

$$\dot{\varepsilon}_2 + b_0\varepsilon_2 = 0 \tag{30}$$

with $b_0 > 0$ and

$$\varepsilon_2 = T_{em} - T_{em_{ref}} \tag{31}$$

The choice of b_0 is detailed in Appendix C. Combining Eqs. (23), (30) and (31), the second new control input u_q is

$$u_q = \dot{T}_{em_{ref}} - a_0(T_{em} - T_{em_{ref}}) \tag{32}$$

the final value of the quadrature rotor voltage component v_{rq} is therefore obtained by replacing u_q expression in Eq. (25) by the above value of u_q in Eq. (32). The DFIG nonlinear state feedback controller with asymptotic output tracking controller scheme is given in Fig. 5.

3.2. Predictive aeroturbine controller

Consider the continuous-time one mass model of the aeroturbine in Eq. (8). The rotors speed is expressed in the Laplace domain as

$$\omega_t(s) = G_T(s)T_a(s) - G_T(s)T_{em}(s) \tag{33}$$

with

$$G_T(s) = \frac{1/K_{t_{hs}}}{(J_{t_{hs}}/K_{t_{hs}})s + 1} \tag{34}$$

In order to use sampled-time predictive control algorithms, a discrete-time input–output representation $G_{T_d}(z^{-1})$ of the aeroturbine is

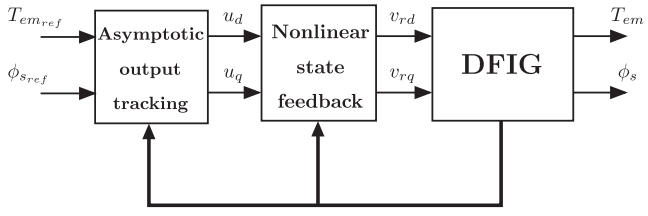

Fig. 5. DFIG nonlinear controller.

obtained. The $G_{T_d}(z^{-1})$ is obtained using the $\mathscr{Z}$-transform.

$$G_{T_d}(z^{-1}) = \frac{(1-e^{-a_t T_s})}{K_{t_{hs}}} \cdot \frac{z^{-1}}{(1-e^{-a_t T_s} z^{-1})} \tag{35}$$

where $a_t = J_{t_{hs}}/K_{t_{hs}}$. In the sampled-time model, $u(k) = T_{em}(k)$ is the control input. The aerodynamic torque $T_a(k)$ is seen as a measurable disturbance input. The rotor speed $y(k) = \omega_t(k)$ is the output. In order to track the optimal rotor speed reference $\omega_{t_{opt}}$, at instant k, a sequence $U(k)$ of control inputs is calculated.

$$\begin{aligned} U_k^T &= [u(1) \ \cdots \ u(m)] \\ &= [\Delta T_{em}(k|k) \ \ \Delta T_{em}(k+1|k) \ \ \cdots \ \ \Delta T_{em}(k+m-1|k)] \end{aligned}$$

where m is the control horizon. The objective is to optimize a cost function $J(U_k)$. It is given by

$$J(U_k) = J_y(U_k) + J_u(U_k) + J_{\Delta u}(U_k) + J_\varepsilon(U_k) \tag{36}$$

Each term takes into consideration a specific objective:

1. For reference tracking

$$J_y(U_k) = \sum_{i=1}^{p} w_i [\omega_{r,ref}(k+i|k) - \omega_r(k+i|k)]^2 \tag{37}$$

2. For control input move suppression

$$J_{\Delta u}(U_k) = \sum_{i=1}^{p-1} w_i^{\Delta u} [T_{em}(k+i|k) - T_{em}(k+i-1|k)]^2 \tag{38}$$

3. and for constraints violation

$$J_\varepsilon(U_k) = \nu \varepsilon_k^2 \tag{39}$$

During the optimization of the criterion $J(U_k)$, a constraint is made upon the maximum value of the inputs

$$|u_k| < u_{max}, \qquad 1 \leqslant k \leqslant m$$

The vector U_k is calculated in order to optimize the criterion $J(U_k)$ while respecting the constraints. This vector is recalculated for each sampling time. The optimization is done using quadratic programming algorithms implemented in Matlab Model Predictive Control Toolbox [51]. The solver is the Dantzig-Wolfe's algorithm [52,53] implemented in the `qpdantz` Matlab function. Once the control sequence vector U_k is obtained, only its first component $u(k)$ is used. The cost function $J(U_k)$ is not convex. Therefore, the convergence to a global minimum is not guaranteed. The algorithm converges generally to a local minimum. However, a local minimum is generally sufficient to achieve control objectives.

3.3. Global controller

The global controller scheme is represented in Fig. 6. It is composed of the interconnection of the DFIG nonlinear controller and the aeroturbine MPC controller. The global controller contains two overlapping loops: an internal and an external loop. The DFIG controller loop is the internal control loop and the predictive aeroturbine controller the external one. This external loop is designed as described in Section 3.2. It must have a time constant of about 0.5 s. As it will be detailed in Section 4.2, the DFIG internal loop has a time constant of 10 ms. That is 50 times much faster compared to the external MPC aeroturbine controller loop. The external MPC control loop gives the references $T_{em_{ref}}$ and $\phi_{s_{ref}}$ to the internal DFIG control loop. Once the references obtained, the DFIG controller computes the control inputs of the DFIG v_{rd} and v_{rq} . The objective is to make T_{em} and ϕ_s very close to their references. The time response of the internal control loop is very short compared to the external one. For the MPC controller design, one can then consider that $T_{em} = T_{em_{ref}}$ and $\phi_s = \phi_{s_{ref}}$. This is depicted in the previous section. The details of the controllers parameter's choice are given in the next simulations section.

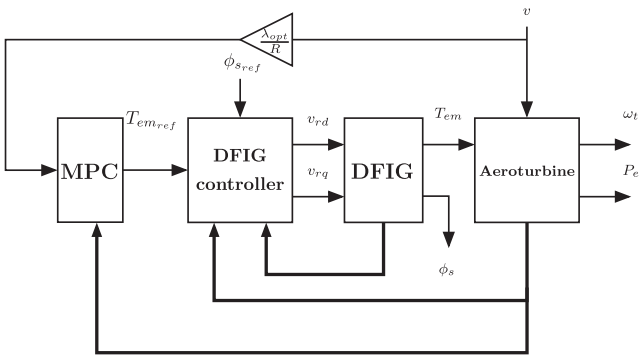

Fig. 6. Global controller.

4. Simulation results

In these section, the simulation procedure is described. After that, the DFIG controller is designed. For comparison, some conventional controllers are briefly presented. The MPC controller is then designed. The performance of the controllers are compared upon the simulation results. A justification is then given for the better MPC controller performances.

4.1. Simulation procedure description

The simulations are carried out with the parameters of the Controls Advanced Research Turbine (CART). This one is located at the NREL [1]. The CART is a two-bladed variable speed, variable pitch experimental wind turbine. It has a nominal power of 600 kW. It is equipped with a three-phase asynchronous generator. This wind turbine is used as the complete set of its parameters is available (aerodynamics, mechanics). However, the proposed approach is valid with a three-bladed wind turbine. The recently installed wind turbine are indeed high-power ones (around 5 MW). However, the proposed controllers can be applied to large-scale wind turbines. The structure and control algorithms do not change. Nevertheless, the parameters (bandwidths, coefficients) must be changed. In fact, a large-scale wind turbine must turn slower than a medium-scale wind turbine. It can instead provide greater control efforts.

The CART parameters are summarized in Table 1 The wind speed profiles used to test the controller are generated using SNWind [54]. It is a wind simulator developed by the NREL. SNWind includes parametrization files for the Turbine/model specifications and the Meteorological Boundary Conditions. In a simple way, the used wind speed can be seen as the sum of two components

$$v = v_m + v_t \tag{40}$$

where v_m is the mean wind speed and v_t the turbulent component. According to Van der Hoven's wind speed spectrum [1], the mean wind speed v_m has a slow variation with a period between 10 min and 2 h. For this, the wind speed profile used during the simulation is of 600 s (10 min). The wind speed profile used to test the MPC controller is shown in Fig. 7. It consists of a set of 600 s data. It is generated using Class-A Kaimal turbulence spectra [55]. The wind profile has a mean value of 7 m/s at the hub height and turbulence intensity of 25%.

[1] NREL (National Renewable Energy Laboratory), Golden, CO.

Table 1
Wind turbine characteristics.

Blade rotor R	21.65 m
Rotor total inertia J_t	392,000 kg·m^2
Aeroturbine damping K_t	400 N·m·rad^{-1}·s
Air density ρ	1.0308 kg/m^3
Gearbox ratio n_g	43.165
Hub height	36.6 m
Maximum rotor torque $T_{g_{max}}$	162 kN·m
Generator system electrical power	600 kW

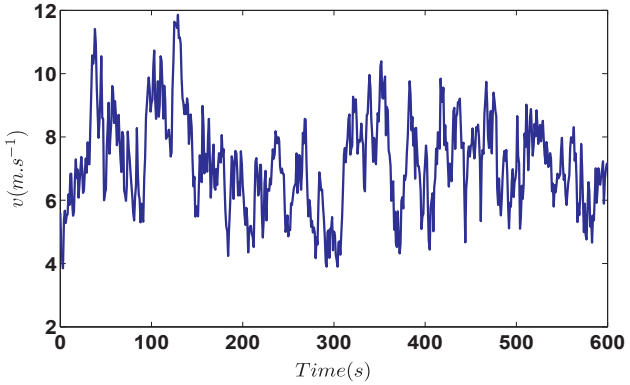

Fig. 7. Wind speed profile.

4.2. DFIG controller design

The aim of the nonlinear DFIG controller is to make an efficient tracking of the stator flux ϕ_s and electromagnetic torque T_{em}. Their references are given by the higher MPC control loop of the aeroturbine. The controlled DFIG dynamics should be very short in comparison to the MPC controller. For this, the DIFG time constant is chosen 50 times faster. It is fixed to 10 ms. The constants a_1,a_0 and b_0 are chosen to meet a 2% settling time t_s of 10 ms. See Appendix A for calculus details. This gives the following values for the tuning parameters

$a_0 = 640 \times 10^3 \quad ; \quad a_1 = 800$
$b_0 = 400.$

The stator flux reference value is fixed to 2 Wb. The simulation results for the stator flux transient are presented in Fig. 8. The flux curve reaches the reference of 2 Wb. As expected, the settling time is about 10 ms. There is no static error. The overshoot is about 8%. The electromagnetic torque transient is depicted in Fig. 9. It presents a good tracking performance of the reference torque $T_{em_{ref}}$.

4.3. Conventional aeroturbine controllers

For comparison with the MPC controller, two other control strategies are briefly described: A conventional PID controller and an LQG controller. Similarly, the objective is to optimize wind power capture.

4.3.1. PID controller

Several design methods are tested to obtain the best PID tunning. Ziegler-Nichols methods in open loop and internal model based technics are tested. They give a tunning that leads to a quickly stalling of the aeroturbine (after few seconds). The best PID controller is obtained with the singular frequency based technique [56]. The obtained PID controller with a derivative filter is given by its transfer function $PID(s)$

$$PID(s) = \frac{2.29{\cdot}10^4 s^2 - 162.3s + 49.99}{s^2 + 10s} \tag{41}$$

4.3.2. LQG controller

The predictive controller is also compared to the LQG controller presented in [57]. For this, a linearized state-space model of the wind turbine is obtained [57]

$$\begin{cases} \dot{x} = Ax + B_1 T'_{em} + B'v' \\ y = Cx \end{cases} \tag{42}$$

$x = [\omega_t' \quad \omega_g' \quad T_{ls}']^T, \; y = \omega_g'$

all the state, input and output variable are defined around their operating point:

$\alpha' = \alpha' - \alpha_0$

where α is any two-mass wind turbine model variable. The following criterion is minimized

$J = \lim_{t\to\infty} \frac{1}{T} \int_0^T x_a^T Q_{x_a} x_a + Q_t (T'_{em})^2 dt$

where x_a is an extended state-space vector

$\mathbf{x}_a = [\omega_t' \quad \omega_g' \quad T_{ls}' \quad v' \quad \dot{v}']^T$

The aim is to ensure power capture optimization while reducing transient loads. The reader is referred to [57] for the complete details about this controller.

4.4. MPC controller design

The MPC controller is designed using the model of the aeroturbine given in Eq. (35). The numerical value of the sampled-time transfer function is

$$G_{T_d}(z^{-1}) = \frac{0.0004743 z^{-1}}{(1 - 0.9956 z^{-1})}$$

and the sampling period is 0.1 s. The choice of the weights of the cost function (36) is made by try-and-error. It leads to the following values

$w_i^{\Delta u} = w^{\Delta u} = 1, \; i = 1,p$
$w_i = w = 1000, \; i = 1,p$
$\nu = 1$

The prediction horizon is fixed to $p = 10$ and the control horizon is fixed to $m = 2$. The MPC controller is designed with the `mpc` function using the Matlab Model Predictive Toolbox [51]. The controller bandwidth is chosen to make a compromise. It is a matter of finding a mid position between power capture maximization and loads reduction. This bandwidth choice allows to track the mean tendency of the optimal rotor speed. It guarantees an efficient capture of wind power without tracking the high turbulences. In fact, tracking turbulence causes fatigue to the wind turbine. The simulation results with the obtained MPC controller are depicted in Figs. 10–14. The rotor speed ω_t

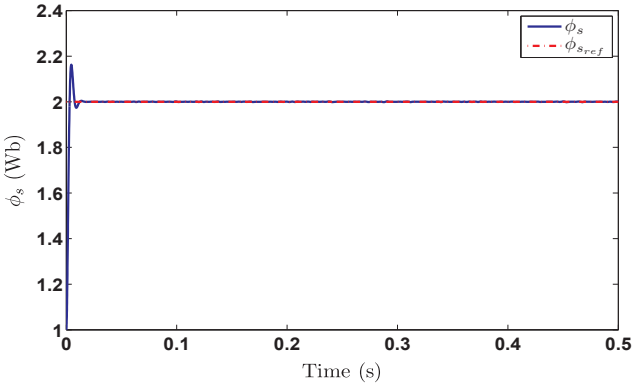

Fig. 8. Transient stator flux.

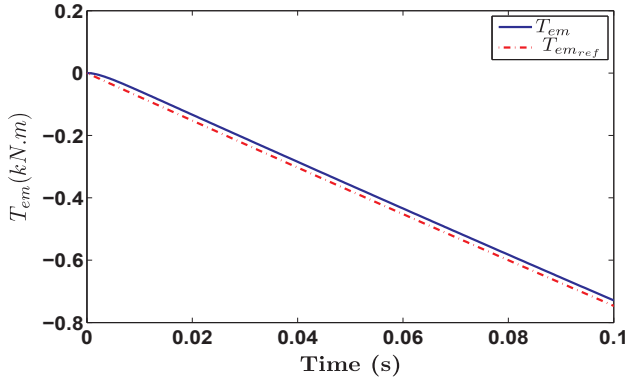

Fig. 9. Transient generator torque.

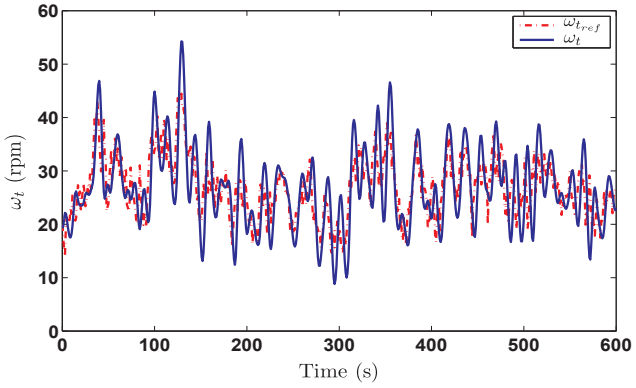

Fig. 10. Rotor speed.

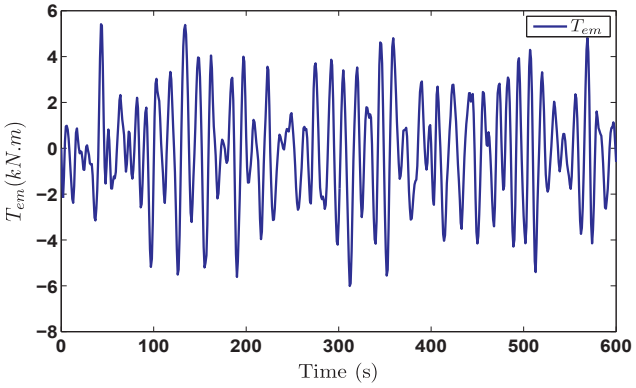

Fig. 11. Generator torque.

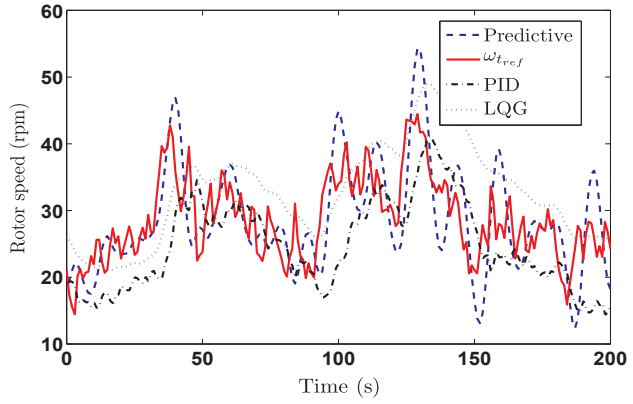

Fig. 12. Comparison of PID and predictive controllers for rotor speed tracking.

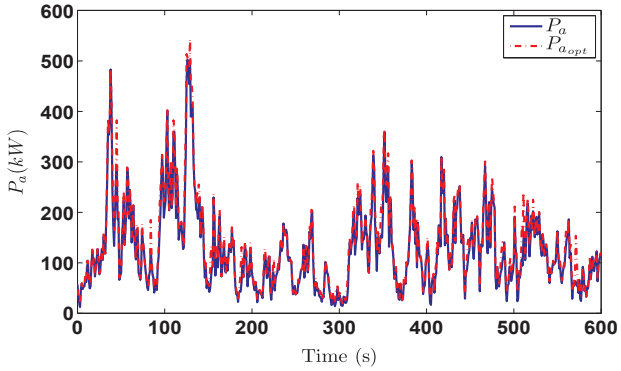

Fig. 13. Aerodynamic power.

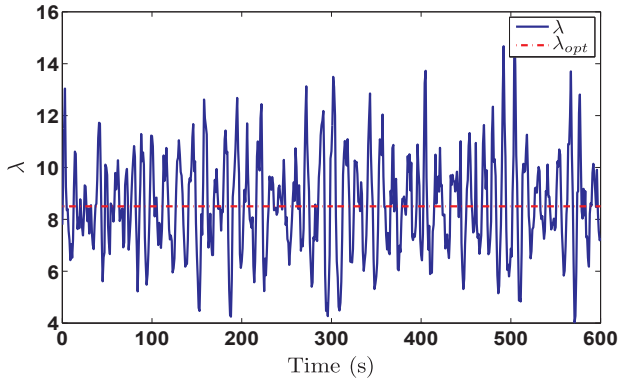

Fig. 14. Tip speed ratio.

and the optimal rotor speed $\omega_{t_{ref}}$ are shown in Fig. 10. The rotor speed tracks the mean tendency of the optimal rotor speed. Its however avoid to track the high-speed variations of the optimal reference. This allows an acceptable control torque T_{em} as shown in Fig. 11. It presents a smooth shape compared to the wind speed.

4.5. Aeroturbine controllers comparison

The proposed predictive controller is compared to the conventional PID controller and the LQG controller. The comparison for the rotor speed tracking is given in Fig. 12. One can see that the predictive controller tracks more closely the optimal rotor speed ω_{ref} while remaining smooth. The rotor speed with the PID and LQG controllers are farther from ω_{ref}. In order to test the efficiency of the controller against wind energy capture, the captured aerodynamic power P_a and the optimal aerodynamic power $P_{a_{opt}}$ are compared. The comparison is shwon in Table 2. These powers expressions are given by

$$P_a = \frac{1}{2}\rho_{air}\pi R^2 C_p(\lambda,\beta_p)v^3 \tag{43}$$

and

$$P_{a_{opt}} = \frac{1}{2}\rho_{air}\pi R^2 C_{p_{opt}} v^3 \tag{44}$$

where $C_{p_{opt}}$ is the optimal value of the power coefficient $C_p(\lambda,\beta_p)$. It is a characteristic of each wind turbine. In the case of the CART wind turbine used in this work, the power curve characteristics are

Table 2
Comparison of power captures.

Controller	*PID*	*LQG*	*Predictive*
$E_{aero}(\%)$	87%	90%	93%

$C_{P_{opt}} = 0.4291 \quad ; \quad \lambda_{opt} = 8.5 \quad ; \quad \beta_{P_{opt}} = 1°$

For a numerical evaluation of the wind power capture efficiency, the aerodynamic efficiency E_{aero} is defined as

$$E_{aero}(\%) = \frac{\int_0^{600} P_a(t)dt}{\int_0^{600} P_{a_{opt}}(t)dt} \times 100(\%) \tag{45}$$

it is the ratio between the total energy captured divided by the optimal energy available. As seen in Table 2, the efficiency of the PID controller is about 87%. The LQG controller efficiency is 90%. Even if the LQG controller surpasses the PID performances, it stand below the predictive controller. As shown in Table 2, the power capture efficiency of the predictive controller is about 93%. That is 3% higher than the LQG and 6% higher than the PID.

The captured aerodynamic power P_a with the predictive controller is depicted in Fig. 13. The optimal aerodynamic power $P_{a_{opt}}$ is shown in the same figure. From this figure, one can see that the captured aerodynamic power is very close to the optimal value. Either the rotor speed ω_t does not track very closely the optimal rotor speed, the aerodynamic power tracks in a better way its optimal value. This is due to a flat shape at the top of the aerodynamic power coefficient $C_p(\lambda,\beta_p)$ curve. Similarly, the tip speed ratio λ, represented in Fig. 14 stands around its optimal value λ_{opt}. It shows a turbulent variation caused by the wind turbulence. With the used wind speed profile, the aerodynamic efficiency is about $E_{aero} = 93\%$. Only 7% of the wind power is lost. This proves the efficiency of the controller.

4.6. Predictive controller performance justification

The good performances of the predictive controller can be explained by two reasons:

1. Firstly, the predictive control scheme is well adapted for systems such as wind turbines. In fact, in predictive control design procedure, a secondary input that is a white gaussian noise is assumed [58]. It is also shown that the wind speed spectral characteristics can be approximated by a filtered white gaussian. This is obtained noise using ARIMA models [59].
2. Secondly, the predictive controller anticipate the adjustment of the control action. This is important because of the great inertia of the wind turbine. In fact, it induces a slow dynamics. Prediction is then essential to deals with the high-rate variations in wind speed profile. It allows to track conveniently the future optimal trajectory. The predictive controller anticipate the adjustment of the control action in order to obtain a smooth control signal and improve power capture.

5. Conclusion

A global controller for both the generator and aeroturbine is proposed. It is applied for a variable speed wind turbine equipped with a DFIG generator. The controller is composed of a nonlinear controller for the DFIG and an MPC controller for the power capture optimization. The two controllers are interconnected using a two-loop control structure with suitable time constants. The simulations are made with the parameters of a real wind turbine and a realistic wind speed profile. They confirm the efficiency of the controller in terms of power capture optimization and control loads reduction. The good performance of the predictive controller are explained by the well adaptation of predictive control scheme for systems like wind turbines. The wind is considered as an filtered-input disturbance. The predictive behavior of the MPC controller allows a premature reaction of the controller for a smooth control of a inertial systems like wind turbine. The predictive controller achieves a good compromise between simplicity and efficiency. A whole controller is to be considered in future works. It will include full load area for high wind speed. It should also take into consideration the transition between power capture optimization and power regulation.

Acknowledgment

The authors would like to thank Ms. Nassima BERKANI for reading the article and the linguistic corrections that have been made.

Appendix A. Wind turbine parameters values

See Tables A.3 and A.4.

Table A.3
Aeroturbine parameters.

Blade rotor R	21.65 m
Air density ρ_{air}	1.308 kg·m^{-3}
High-speed equivalent inertia $J_{t_{hs}}$	210.3888 kg·m^2
High-speed equivalent damping $K_{t_{hs}}$	9.2668 N·m·rad^{-1}·s^{-1}

Table A.4
DFIG parameters.

Rotor resistance R_r	0.0061 Ω
Stator resistance R_s	0.0069 Ω
L_s	0.0068 H
L_r	0.0068 H
M	0.0067 H

Appendix B. Direct axis stator voltage v_{sd} time derivative

The stator voltage direct component v_{sq} in (d,q) reference frame is

$$v_{sd} = [\cos\rho \quad \sin\rho]\begin{bmatrix} v_{s\alpha} \\ v_{s\beta} \end{bmatrix} \tag{B.1}$$

where (α,β) is a fixed reference frame and ρ the angular position of the d,q reference frame to the (α,β) one. The (α,β) stator voltage components are

obtained by the Concordia transformation from the natural 3-phases reference frame (a,b,c)

$$\begin{bmatrix} v_{s\alpha} \\ v_{s\beta} \end{bmatrix} = \underbrace{\sqrt{\frac{2}{3}} \begin{bmatrix} 1 & -\frac{1}{2} & -\frac{1}{2} \\ 0 & \sqrt{\frac{3}{2}} & -\sqrt{\frac{3}{2}} \end{bmatrix}}_{C} \begin{bmatrix} v_{sa} \\ v_{sb} \\ v_{sc} \end{bmatrix} \tag{B.2}$$

where C is the Concordia matrix and $\begin{bmatrix} v_{sa} \\ v_{sb} \\ v_{sc} \end{bmatrix}$ the natural 3-phases stator voltage

$$\begin{bmatrix} v_{sa} \\ v_{sb} \\ v_{sc} \end{bmatrix} = V_{\max} \begin{bmatrix} \sin(\omega t) \\ \sin(\omega t - \frac{2\pi}{3}) \\ \sin(\omega t - \frac{4\pi}{3}) \end{bmatrix} \tag{B.3}$$

By usual time derivative properties for scalars, vectors and matrix [60] and using the time derivative of ρ given by Eq. (11), after simplification, the time derivative of the direct component stator flux voltage in (d,q) reference frame is

$$\frac{dv_{sd}}{dt} = [v_{sa} \quad v_{sb} \quad v_{sc}] C^T \frac{M\alpha i_{rq} + v_{sq}}{\phi_{sd}} \begin{bmatrix} -\sin\rho \\ \cos\rho \end{bmatrix} + [\cos\rho \quad \sin\rho] C\omega V_{\max} \begin{bmatrix} \sin(\omega t + \frac{\pi}{2}) \\ \sin(\omega t - \frac{\pi}{6}) \\ \sin(\omega t - \frac{5\pi}{6}) \end{bmatrix}. \tag{B.4}$$

with

$$\cos\rho = \frac{\phi_{s\alpha}}{\sqrt{\phi_{s\alpha}^2 + \phi_{s\beta}^2}} \quad ; \quad \sin\rho = \frac{\phi_{s\beta}}{\sqrt{\phi_{s\alpha}^2 + \phi_{s\beta}^2}}$$

Appendix C. DIFG Controller parameters design

The coefficients a_i are found by identification of the corresponding Hurwitz polynomial to a standard second order polynomial. It involves the damping coefficient ξ and the crossover frequency ω_0, namely:

$$s^2 + a_1 s + a_0 = s^2 + 2\xi\omega_0 s + \omega_0^2$$

leading to

$$a_0 = \omega_0^2$$
$$a_1 = 2\xi\omega_0$$

as $\omega_0 \approx \frac{4}{\xi t_r}$, where t_r is the 2% setting time and ξ the damping coefficient [61].

References

[1] Burton T, Jenkins N, Sharpe D, Bossanyi E. Wind energy handbook. 2nd ed. Wiley; 2011.
[2] Hird M. Wind energy literature survey no. 1. Wind Energy 2000;3(3):165–6.
[3] Henriksen LC. Wind energy literature survey no. 32. Wind Energy 2014;17(8):1297–300.
[4] Njiri JG, Söffker D. State-of-the-art in wind turbine control: Trends and challenges. Renew Sustain Energy Rev 2016;60:377–93.
[5] Boukhezzar B. Sur les stratégies de commande pour l'optimisation et la régulation de puissance des éoliennes à vitesse variable Ph.D. thesis Université Paris Sud-Paris XI; 2006.
[6] Heier S. Grid integration of wind energy: onshore and offshore conversion systems. John Wiley & Sons; 2014.
[7] Hur S, Leithead W. Model predictive and linear quadratic gaussian control of a wind turbine. Optimal Control Appl Methods 2017;38(1):88–111.
[8] Fragoso S, Garrido J, Vázquez F, Morilla F. Comparative analysis of decoupling control methodologies and h_∞ multivariable robust control for variable-speed, variable-pitch wind turbines: Application to a lab-scale wind turbine. Sustainability 2017;9(5):713.
[9] Bianchi FD, Batista HD, Mantz RJ. Wind turbine control systems: principles, modelling and gain scheduling design (advances in industrial control). Springer; 2006.
[10] Østergaard KZ. Robust, gain-scheduled control of wind turbines Ph.D. thesis Automation and Control, Department of Electronic Systems, Aalborg University; 2008.
[11] Kazmi SMR, Goto H, Guo H-J, Ichinokura O. A novel algorithm for fast and efficient speed-sensorless maximum power point tracking in wind energy conversion systems. IEEE Trans Ind Electron 2011;58(1):29–36.
[12] Muhando E, Senjyu T, Yona A, Kinjo H, Funabashi T. Disturbance rejection by dual pitch control and self-tuning regulator for wind turbine generator parametric uncertainty compensation. IET Control Theory Appl 2007;1(5):1431–40.
[13] Mechter A, Kemih K, Ghanes M. Backstepping control of a wind turbine for low wind speeds. Nonlinear Dyn 2016;84(4):2435–45.
[14] Leonhard W. Control of electrical drives. Springer Science & Business Media; 2012.
[15] Abad G, Lopez J, Rodriguez M, Marroyo L, Iwanski G. Doubly fed induction machine: modeling and control for wind energy generation vol. 85. John Wiley & Sons; 2011.
[16] Xu L, Cartwright P. Direct active and reactive power control of DFIG for wind energy generation. IEEE Trans energy Convers 2006;21(3):750–8.
[17] Boukhezzar B, Siguerdidjane H. Nonlinear control with wind estimation of a DFIG variable speed wind turbine for power capture optimization. Energy Convers Manage 2009;50(4):885–92.
[18] Phan D-C, Yamamoto S. Rotor speed control of doubly fed induction generator wind turbines using adaptive maximum power point tracking. Energy 2016;111:377–88.
[19] Evangelista C, Valenciaga F, Puleston P. Active and reactive power control for wind turbine based on a mimo 2-sliding mode algorithm with variable gains. IEEE Trans Energy Convers 2013;28(3):682–9.
[20] Xiong P, Sun D. Backstepping-based DPC strategy of a wind turbine-driven DFIG under normal and harmonic grid voltage. IEEE Trans Power Electron 2016;31(6):4216–25.
[21] Yang B, Yu T, Shu H, Dong J, Jiang L. Robust sliding-mode control of wind energy conversion systems for optimal power extraction via nonlinear perturbation observers. Appl Energy 2018.
[22] Qin SJ, Badgwell TA. A survey of industrial model predictive control technology. Control Eng Practice 2003;11(7):733–64.
[23] Sultana WR, Sahoo SK, Sukchai S, Yamuna S, Venkatesh D. A review on state of art development of model predictive control for renewable energy applications. Renew Sustain Energy Rev 2017;76:391–406.
[24] Yaramasu V, Wu B. Model predictive decoupled active and reactive power control for high-power grid-connected four-level diode-clamped inverters. IEEE Trans Industr Electron 2014;61(7):3407–16.
[25] Liu X, Kong X. Nonlinear model predictive control for DFIG-based wind power generation. IEEE Trans Autom Sci Eng 2014;11(4):1046–55.
[26] Darabian M, Jalilvand A. Predictive control strategy to improve stability of DFIG-based wind generation connected to a large-scale power system. Int Trans Electrical Energy Syst 2017;25(5).
[27] Song D, Yang J, Dong M, Joo YH. Model predictive control with finite control set for variable-speed wind turbines. Energy 2017;126:564–72.
[28] Odgaard PF, Larsen LF, Wisniewski R, Hovgaard TG. On using Pareto optimality to

tune a linear model predictive controller for wind turbines. Renew Energy 2016;87:884–91.
[29] Varzaneh SG, Abedi M, Gharehpetian G. A new simplified model for assessment of power variation of DFIG-based wind farm participating in frequency control system. Electric Power Syst Res 2017;148:220–9.
[30] Poitiers F. Etude et commande de génératrices asynchrones pour l'utilisation de l'energie eolienne, Ph.D. thesis, Ecole Polytechnique de l'Université de Nantes; December 2003.
[31] Kalamian N, Verij Kazemi M, Gholomian SA. Direct power control of DFIG by using nonlinear model predictive controller. Asian J Control 2016;18(3):985–99.
[32] Wilkie J, Leithead W, Anderson C. Modelling of wind turbines by simple models. Wind Eng 1990;14(4):247–74.
[33] El Aimani S. Modélisation des différentes technologies d'éoliennes intégrées dans un réseau de moyenne tension Ph.D. thesis Ecole Centrale de Lille; 2004.
[34] Boukhezzar B, Siguerdidjane H. Nonlinear control of a variable-speed wind turbine using a two-mass model. IEEE Trans Energy Convers 2011;26(1):149–62.
[35] Boukezzar B, M'Saad M. Robust sliding mode control of a DFIG variable speed wind turbine for power production optimization. Control and automation, 2008 16th mediterranean conference on. IEEE; 2008. p. 795–800.
[36] Hansen LH, Helle L, Blaabjerg F, Ritchie E, Munk-Nielsen S, Bindner HW, et al. Conceptual survey of generators and power electronics for wind turbines. Tech Rep, Risø; 2002.
[37] Muller S, Deicke M, De Doncker RW. Doubly fed induction generator systems for wind turbines. IEEE Ind Appl Mag 2002;8(3):26–33.
[38] Björnstedt J. Integration of non-synchronous generator frequency dynamics Ph.D. thesis Sweden: Lund University; 2012.
[39] Majumder R, Ghosh A, Ledwich G, Zare F. Power management and power flow control with back-to-back converters in a utility connected microgrid. IEEE Trans Power Syst 2010;25(2):821–34.
[40] Srirattanawichaikul W, Premrudeepreechacharn S, Kumsuwan Y. A comparative study of vector control strategies for rotor-side converter of DFIG wind energy systems. Electrical engineering/electronics, computer, telecommunications and information Technology (ECTI-CON), 2016 13th international conference on. IEEE; 2016. p. 1–6.
[41] Malesani L, Rossetto L, Tenti P, Tomasin P. Ac/dc/ac PWM converter with reduced energy storage in the dc link. IEEE Trans Ind Appl 1995;31(2):287–92.
[42] Sira-Ramírez H, Silva-Ortigoza R. Control design techniques in power electronics devices. Springer Science & Business Media; 2006.
[43] Bequette BW. Process control: modeling, design, and simulation. Prentice Hall Professional; 2003.
[44] Marino R, Tomei P, Verrelli CM. Induction motor control design. Springer Science & Business Media; 2010.
[45] Chen Z, Yin M, Zou Y, Meng K, Dong Z. Maximum wind energy extraction for variable speed wind turbines with slow dynamic behavior. IEEE Trans Power Syst 2017;32(4):3321–2.
[46] Chen W-H, Chen C-Y, Huang C-Y, Hwang C-J. Power output analysis and optimization of two straight-bladed vertical-axis wind turbines. Appl Energy 2017;185:223–32.
[47] Mohammadi J, Vaez-Zadeh S, Afsharnia S, Daryabeigi E. A combined vector and direct power control for DFIG-based wind turbines. IEEE Trans Sustain Energy 2014;5(3):767–75.
[48] Slootweg JG, de Haan WH, Polinder H, Kling W. General model for representing variable speed wind turbines in power system dynamic simulations. IEEE Trans Energy Convers 2003;18(1):144–50.
[49] Forchetti D, Garcia G, Valla MI. Vector control strategy for a doubly-fed stand-alone induction generator. In: IEEE 2002 28th annual conference of the industrial electronics society; 2002. p. 991–5.
[50] Isidori A. Nonlinear control systems. Springer Science & Business Media; 2013.
[51] Bemporad A, Morari M, Ricker NL. Model predictive control toolbox, user's guide. The Mathworks; 2010.
[52] Fletcher R. Practical methods of optimization. John Wiley & Sons; 2013.
[53] Dantzig G. Linear programming and extensions. Princeton University Press; 2016.
[54] Buhl ML. SNwind USER's GUIDE. 1st ed. Golden, Colorado: National Wind Technology Center, National Renewable Energy Laboratory; 2003.
[55] Peña A, Floors R, Sathe A, Gryning S-E, Wagner R, Courtney MS, et al. Ten years of boundary-layer and wind-power meteorology at høvsøre, denmark. Boundary Layer Meteorol 2016;158(1):1–26.
[56] Dorf RC, Bishop RH. Modern control systems. Pearson; 2011.
[57] Boukhezzar B, Siguerdidjane H. Comparison between linear and nonlinear control strategies for variable speed wind turbines. Control Eng Practice 2010;18(12):1357–68.
[58] Rossiter JA. Model-based predictive control: a practical approach. CRC Press; 2003.
[59] Chen P, Pedersen T, Bak-Jensen B, Chen Z. Arima-based time series model of stochastic wind power generation. IEEE Trans Power Syst 2010;25(2):667–76.
[60] Dhrymes PJ. Mathematics for econometrics. Springer; 1978.
[61] Nise NS. Control systems engineering. 6th ed. Wiley; 2011.